Determination of concentration of boron atoms on Ag surface by PGAA

Neutron Physics Laboratory - Nuclear analytical methods with neutrons

Tomáš Baše

Proposal ID

145

Ag films exposed to a methanol solution of isomer 9,12-$(HS)_2$-1,2-$C_2B_{10}H_{10}$ were analyzed using PGAA (Prompt Gamma-ray Activation Analysis) method to determine the concentration of boron. The concentration of nine samples with various exposure time were determined by PGAA. The absolute boron contents in these samples were converted into boron area density as the number of B atoms/cm^2. These results allow us to control the formation of Self-Assembled-Monolayers (SAM) on polycrystalline Ag films with respect to exposure time. They will be used in further development of metal-based materials with tunable physical and chemical properties.

Assessment of the Impact of North Mara Gold Mine on River Mara Fish Contamination by Heavy Metals

Neutron Physics Laboratory - Nuclear analytical methods with neutrons

Najat Mohammed

Proposal ID

40

Samples of catfish (*Clarias mossambicus*) and lungfish (*Protopterus aethiopicus*) which are most consumed species of fish from River Mara in Tarime District of Mara Region were analyzed by INAA. Twenty samples of each fish species were collected from two sampling stations of Wegita (downstream) and Mrito (upstream) along River Mara at vicinity of North Mara Gold Mine (NMGM). The sampling stations were 70 km apart.
The samples were freeze dried, homogenized by cryogenic grinding and deep-frozen prior to analysis. Sample aliquots of approximately 100 mg and 200 mg for short-time and long-time irradiation, respectively, were sealed into acid-cleaned polyethylene disk-shaped capsules. Short- and long-time irradiations for 30 s and 3 h, respectively, were carried out in the LVR-15 reactor of the Research Centre Řež, Ltd. at neutron fluence rates of $3 \cdot 10^{13}$ cm^2 s^{-1}, $1 \cdot 10^{13}$ cm^2 s^{-1} , and $8 \cdot 10^{13}$ cm^2 s^{-1} for thermal, epithermal, and fast neutrons, respectively. Multielement standards containing known amounts of elements to be determined were simultaneously irradiated with the samples. For quality control purposes, NIST SRM 1577b Bovine Liver and NIST SRM 2711 Montana Soil were analyzed.

Counting of the irradiated samples and standards was performed in conditions given in Table 1, where t_i is irradiation time, t_d is decay time, t_c is counting time, and counting geometry is the distance of the sample from the cap of the detector. The samples and multielement standards were counted in the same geometry.

Table 1. Irradiation and counting conditions

t_i	t_d	t_c	Counting geometry	Detector[a]
30 s	10 min.	10 min.	15 cm	HPGe-1
3 h	4-5 days	1 h	20 cm	HPGe-2
	1 month	3 h	1 cm	HPGe-2

[a] HPGe-1: coaxial HPGe detector with 23 % relative efficiency, resolution FWHM 1.80 keV for the 1332.5 keV photons of ^{60}Co

HPGe-2: coaxial HPGe detector with 53 % relative efficiency, resolution FWHM 1.80 keV for the 1332.5 keV photons of ^{60}Co

The detectors were coupled to Canberra Genie 2000 computer-controlled gamma spectrometer via the chain of linear electronics, which contained a loss-free counting module (LFC Canberra 599, dual mode) to correct for the pile-up effect and dynamic changes of dead time.

Fifteen elements which are Na, Cl, K, Ca, Sc, Cr, Mn, Fe, Co, Zn, Se, Br, Rb and Sr were detected in concentration above the Minimum Detection Limit (MDL) in samples of both fish species. The concentrations of toxic elements As, Cd, Th and U were found to be below MDL of the system used in this study. In this project Hg was not detected. Most of the elements were found to be in higher concentrations in samples from downstream than upstream which might indicate contamination from the nearby Gold mine.

Neutron diffraction in welded and fatigued steels

Neutron Physics Laboratory - Neutron diffraction

Evangelos Hristoforou

Proposal ID

71

The present report refers to the determination of the residual stress values along the surface of welded ferromagnetic steels, by using three different techniques: X-ray diffraction, neutron diffraction and magnetic Barkhausen noise. The latter in not an established method for measuring the lattice stains and determining the corresponding stress values.

Three different grades of ferromagnetic steel were tested: (1) non-oriented electrical steel (2) low carbon (mild) steel: AISI 1008 and (3) low alloyed carbon steel: AISI 4130. For each grade of steel, two identical sheets were welded together in a butt joint configuration. The direction of the welding, in NOES samples, was perpendicular to the rolling direction, whereas, in both AISI 1008 and AISI 4130 samples this was parallel to the rolling direction.

Stress measurements on the surface of the test samples were conducted with the Magnetic Barkhausen Noise (MBN) technique, as well as, the X-ray (XRD) and the neutron[1] diffraction methods. The determination of the residual stresses with the neutron diffraction method is not straightforward. The crystal lattice deformations were determined through the relevant measurements on the surface of a polycrystalline material, due to the presence of stress. Then, the residual stresses were calculated by using a suitable mathematical relationship. An example of the ND monitored residual stress distribution on the surface of the welded AISI 1008 sample is shown in Fig. 1. Figure 2 illustrates cross-plotting of the residual stress measurements by MBN, neutron and XRD diffraction on EBW welded AISI 4130 sample and TIG welded AISI 4130 sample

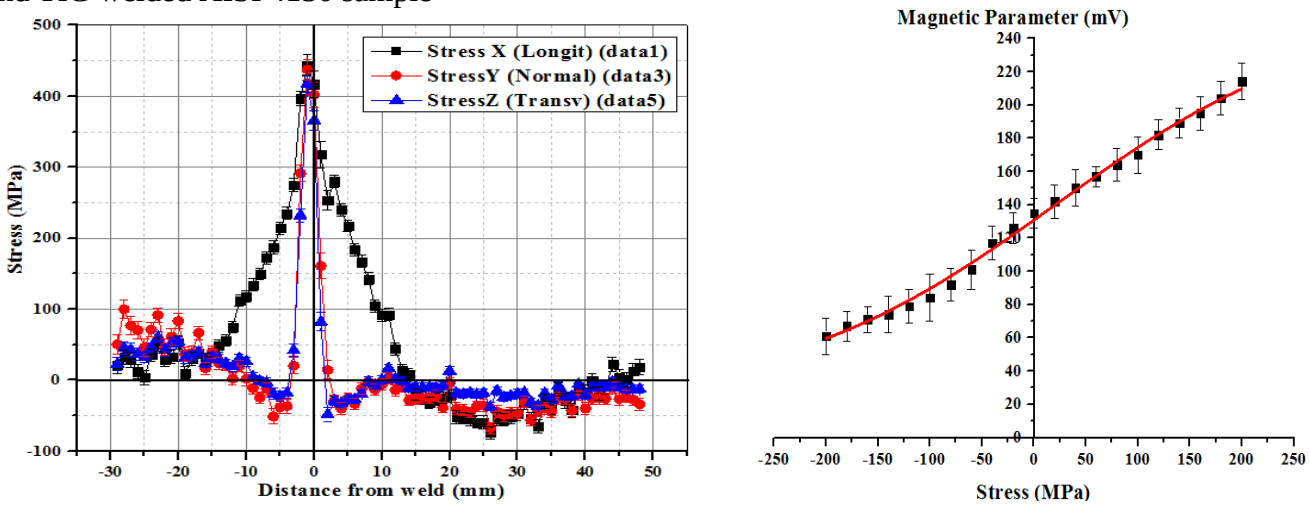

Figure 1: *Distribution of the residual stress values determined by the neutron diffraction measurements, on the surface of the AISI 1008 welded sample (left). Calibration of the stresses against magnetic permeability (right)*

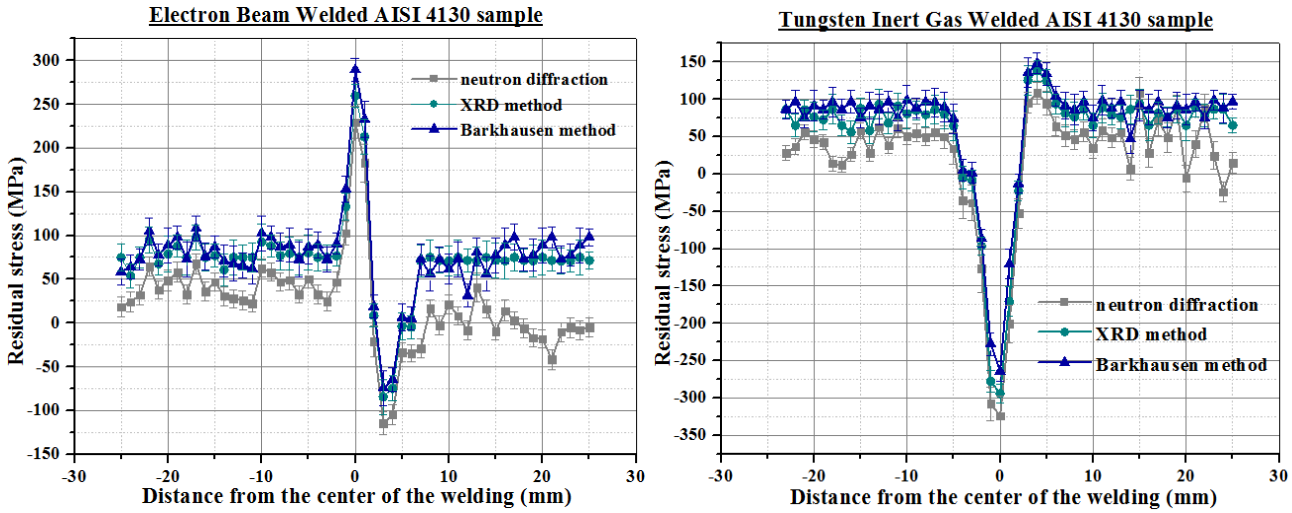

Figure 2: *Cross-plotting of the residual stress measurements by magnetic Barkhausen noise, neutron and XRD diffraction on the EBW welded AISI 4130 sample and (c) TIG welded AISI 4130 sample.*

[1] The low thickness and the dimensions of the welded NOES samples did not allow the measurement of the residual stress with the neutron diffraction method: the determination of the residual stress was conducted with MBN and XRD methods. In the present report, only the experimental results from the welded AISI 1008 and AISI 4130 samples are valid.

Crystal and Magnetic Structures of the Orthorhombic Perovskites LnFe2/3Mo1/3O3 (Ln=La,Ce,Pr,Nd)

Neutron Physics Laboratory - Neutron diffraction

Roland Tellgren

Proposal ID

144

Neutron Diffraction Studies of Orthorhombic Rare-Earth Ferrates
$LnFe_{2/3}Mo_{1/3}O_3$ (Ln=La, Ce, Pr, Nd)

Roland Tellgren and Sergey Ivanov
The Angstrom Laboratory, Uppsala University
Box 538, SE 75121, Uppsala, Sweden

The powder samples were studied at 4K, 300K, 450K and 600K on diffractometer MEREDIT (Rez, Czech Republic) with the wavelength of 1.46 Å. The amount of La and Pr samples was quite low because there were serious problems with preparation of a suitable volume of pure perovskite phases. The NPD experimental diffraction patterns were analyzed with the Rietveld profile method using the FULLPROF program. The diffraction peaks were described by a pseudo-Voigt profile function, with a Lorentzian contribution to the Gaussian peak shape. A peak asymmetry correction was made for angles below 35° (2θ). Background intensities were estimated by interpolating between up to 40 selected points (low temperature NPD experimental data) or described by a polynomial with six coefficients. During the refinements the two *B*-type cations (Fe and Mo) were allowed to vary their occupation on the possible metal sites. The refined atomic coordinates at different temperatures were used to calculate the bond distances and angles. The magnetic propagation vector was determined from the peak positions of the magnetic diffraction lines using the K-search software which is included in the FULLPROF refinement package. Magnetic symmetry analysis was then done using the program BASIREPS, also part of FULLPROF. Several magnetic models were tried in the refinement, each employing one additional refinement parameter, corresponding to the magnitude of the magnetic moment. Each structural model was refined to convergence, with the best result selected on the basis of agreement factors and stability of the refinement.

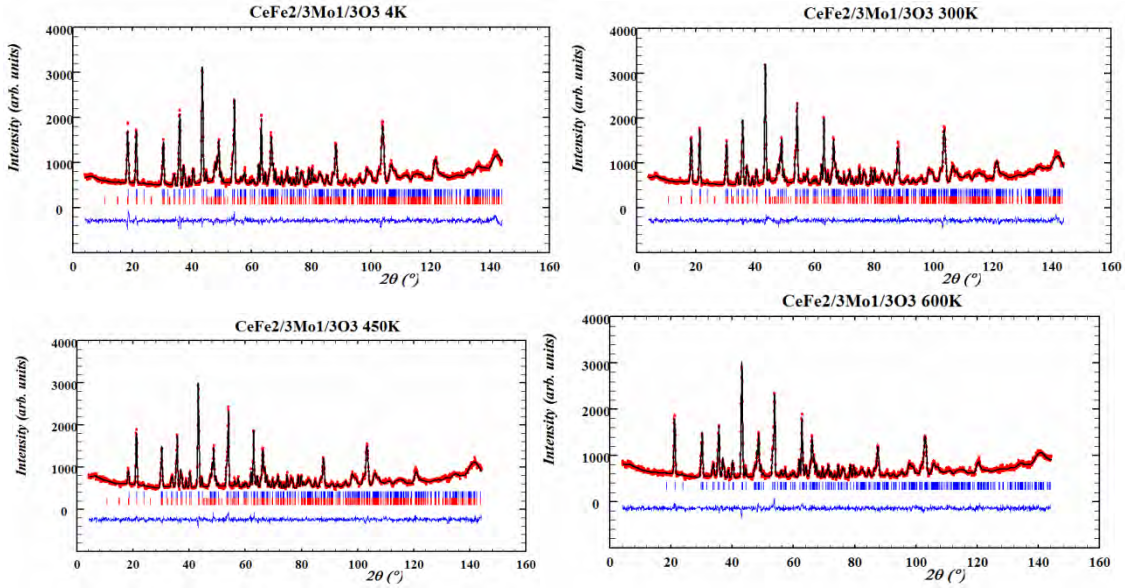

Figure 1. Final Rietveld plots for $CeFe_{2/3}Mo_{1/3}O_3$ obtained for NPD patterns at different temperatures

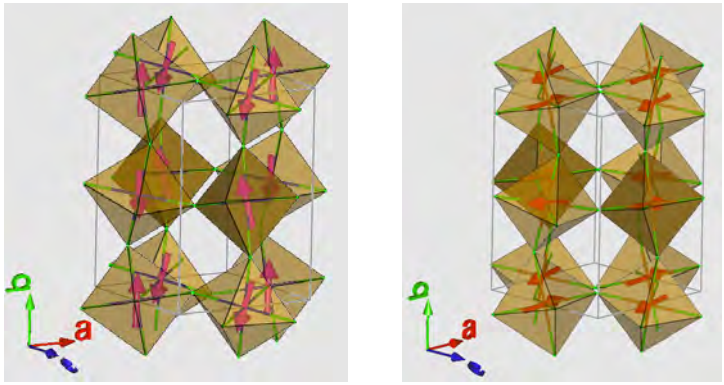

Figure 2. The crystal and G-type magnetic structure for $CeFe_{2/3}Mo_{1/3}O_3$ at 300 and 4 K.

SANS studies of ferroelectrics embedded into magnetic porous glasses

Neutron Physics Laboratory - Neutron diffraction

Aleksandr Naberezhnov

Proposal ID

141

SANS studies of ferroelectrics embedded into magnetic porous glasses.

Instrument MAUD. Experimental team V. Ryukhtin, A. Naberezhnov

We have studied the inner structure of empty microporous (Fe20MIP) and macroporous (Fe20MAP) magnetic glasses and the composites on base of these matrices containing embedded ferroelectrics $NaNO_2$ and KNO_3. These composites are very interesting for creation of so-called artificial multiferroics with spatially separated ferroelectric and magnetic orderings [1-3]. In Figure the results of preliminary analysis of SANS data for the nanocomposites Fe20MIP+$NaNO_2$ and Fe20MIP+KNO_3 are presented. At treatment we have used the approximation of non-interactive spheres with log-normal distributions. The principle results for ferroelectric-containing samples are:

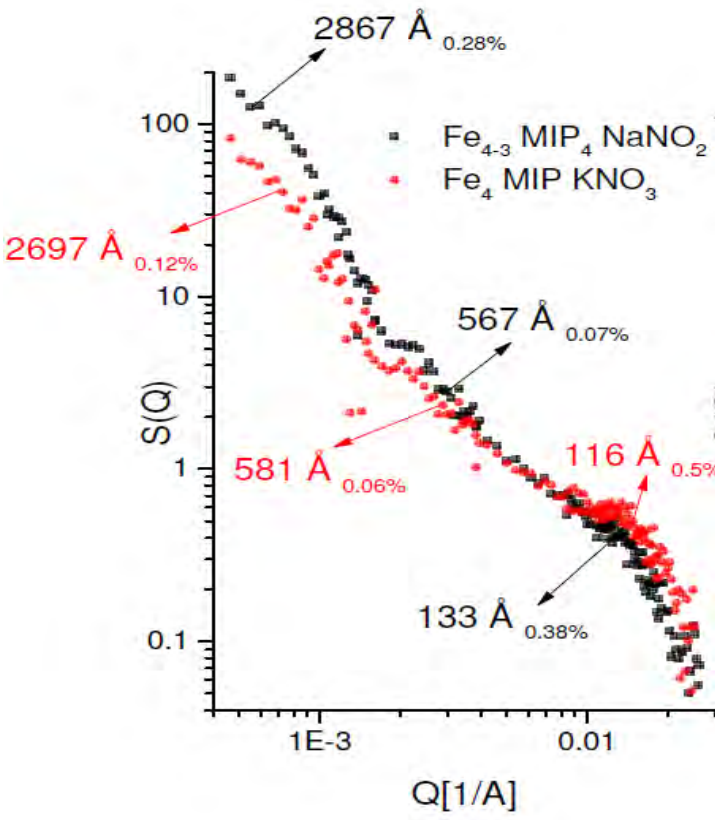

– There are three types of scattering objects with different characteristic sizes. The largest and the smallest objects correspond to the magnetic nanoparticles existing in these magnetic glasses and their sizes are in good agreement with AFM and X-rays diffraction data [4]. The middle size corresponds to the ferroelectric nanonoparticles and confirms the experimental observation that in porous glasses with small average pore diameters the embedded ferroelectrics form the dendrite network of independent clusters with the size essentially larger than average pore diameter (5 nm) in Fe20MIP glasses [5]. It is necessary to note that this results (in common with AFM, magnetic force microscopy, TEM and X-rays data [2-4]) is the first direct evidence of coexistence of two types magnetic particles and ferroelectric nanoclusters distributed in a volume of Fe20MIP and Fe20MAP glasses.

References

1 Manual Bibes, “Nanoferronics is a winning combination” ***Nature Materials*** 11, 354 – 357, (2012)

2 Alexander Naberezhnov et al, “Nanoporous Glasses with Magnetic Properties as a Base of High-frequency Multifunctional Device Making” ***Lecture Notes in Computer Science*** 8638, 459-466 (2014)

3 Alexander Naberezhnov et al., “Morphology and Magnetic Properties of Ferriferous Two-Phase Sodium Borosilicate Glasses” ***The Scientific World Journal***, Volume 2014, Article ID 320451, 7 pages, (2014)

4 T. V. Antropova, I. N. Anfimova, A. A. Naberezhnov et al.,“Structure of Magnetic Nanoclusters in Ferriferous Alkali Borosilicate Glasses” ***Physics of the Solid State***, 54(10), 2110–2115 (2012)

5 S. B. Vakhrushev, I. V. Golosovsky, A. A. Naberezhnov et al., “Structure and Dielectric Response of $Na_{1-x}K_xNO_2$ Nanocomposite Solid Solutions” ***Physics of the Solid State***, 50(8), 1548–1554 (2008)

Determination of minor and trace elements in coal samples from Turkey

Neutron Physics Laboratory - Nuclear analytical methods with neutrons

Sema Erenturk

Proposal ID

20

DETERMINATION OF MAJOR, MINOR, AND TRACE ELEMENTS IN COAL SAMPLES FROM TURKEY

Coal and its combustion by products may contain hazardous elements, therefore power plants that burn coals and disposal sites for wastes from these plants are one of the principal sources of global contamination of soils, waters, and air that effect human health. The goal of this project was determination of major, minor, and trace elements in coal samples used in thermal power plant in Turkey. Coal and its combustion products contain elements, which are principal sources of global contamination of soils, water, and air. As a consequence this contamination effects also the human health and environment.

After receiving the material to be analyzed in Nuclear Physics Institute (11.04.2014) raw coal samples were crushed and grinded in the mill (14.04.2014), sampled in to polyethylene bags with mass approximately 110 mg, and together with SRMs 1547, 2711, 16333B, 1635, and 1632B were prepared for short-time analysis (10.05.2014 and 17.05.2014). Moisture content in samples was determined by drying in the oven for 5 hours in 105°C (24.06.2014 and 10.07.2014)

Short-time analysis was carried out on 20.6.2014 by irradiating the samples for one minute in channel H1. Decay and measurement time was set to 13 min. The same day the samples were packed to aluminum tube for long-time irradiation and irradiated 24.06.2014 for 3 hours in channel H8. Samples were unpacked after three days of decay and measured for the first time for 90 min. Second measurement is planned after one month of the decay for 6 hours. For both measurements detector Canberra is used (77.8%, resolution FWHM 1.87 keV @1332.5 keV, and peak-to Compton ratio of 82.5:1). The detector is connected to a Canberra Genie 2000 γ-spectrometer through a chain of linear electronics, which contained a loss-free counting module (LFC Canberra 599, dual mode) to correct for pile-up effect and dynamic changes of dead time.

Canberra Genie 2000 software is used to control measurements and to evaluate the spectra obtained. Results of k_0-NAA will be calculated using both k0-IAEA program and Kayzero for Windows software. Expected date of delivering complete results to Istanbul Technical University is 15.09.2014.

Surface analysis of plasma and laser modified substrates

Laboratory of Tandetron

Petr Slepika

Proposal ID

35

The following research topics have been studied:

a) Gold nanolayer and nanocluster coatings induced by heat treatment and evaporation technique

The preparation and surface characterization of gold coatings and nanostructures deposited on glass substrate was performed. Different approaches for the layer preparation were applied. The gold was deposited on the glass with (i) room temperature, (ii) glass heated to 300°C, and (iii) the room temperature-deposited glass which was consequently annealed to 300°C. The sheet resistance and concentration of free carriers were determined by the van der Pauw method. Surface morphology was characterized using an atomic force microscopy. The optical properties of gold nanostructures were measured by UV–vis spectroscopy. The evaporation technique combined with simultaneous heating of the glass leads to change of the sheet resistance, surface roughness, and optical properties of gold nanostructures. The electrically continuous layers are formed for significantly higher thickness (18 nm), if the substrate is heated during evaporation process. The annealing process influences both the structure and optical properties of gold nanostructures. The elevated temperature of glass during evaporation amplifies the peak of plasmon resonance in the structures, the surface morphology being significantly altered. The difference in surface metal distribution of evaporated structures under RT and evaporated onto substrate heated to 300°C is evaluated in Figure 1. The difference in the behavior of surface nanostructures in area on electrical discontinuity and continuity can be clearly seen. The electrically discontinuous layer exhibits significantly higher gold concentration when deposited on non-heated substrate. The heat treatment seems to be a positive promoter of surface diffusion (and nanocluster growth), mostly in the early stages of gold layer growth. This difference, thus, seems to affect the surface gold concentration; the higher the surface concentration, the more homogeneous the layer is. On the contrary, for higher gold thicknesses, when the layer is already electrically continuous, this difference is reversed.

b) Biopolymer nanostructures induced by argon plasma irradiation and metal sputtering

Physicochemical properties of polymer surface may be modified by many techniques based on various chemical or physical processes. Modification based on polymer surface exposure to plasma irradiation exhibits an easy and cheap technique for biopolymer surface nanostructuring. By plasma exposure of polymer surface combined with consequent heating or metal deposition can be prepared materials applicable both in tissue engineering as cell carriers, but also in integrated circuit manufacturing. The influence of argon plasma irradiation on PLLA (poly(L-lactide acid) was presented. The combination of Ar+ particle irradiation, consequent sputter metallization and heating of biopolymer surface was summarized. Wettability of modified surface was characterized by the contact angle and surface energy determination. The surface morphology was studied using atomic force microscope and laser confocal microscope. The chemical analysis was performed using Rutherford Backscattering Spectroscopy (RBS) and X-ray Photoelectron Spectroscopy (XPS). The combination of plasma treatment with consequent thermal heating and/or metal sputtering led to the change of surface wettability, morphology and chemical structure. The surface roughness has been strongly influenced by the modification parameters, as well as the surface chemistry of biopolymer. The modification techniques had a positive effect on cell adhesion and proliferation.

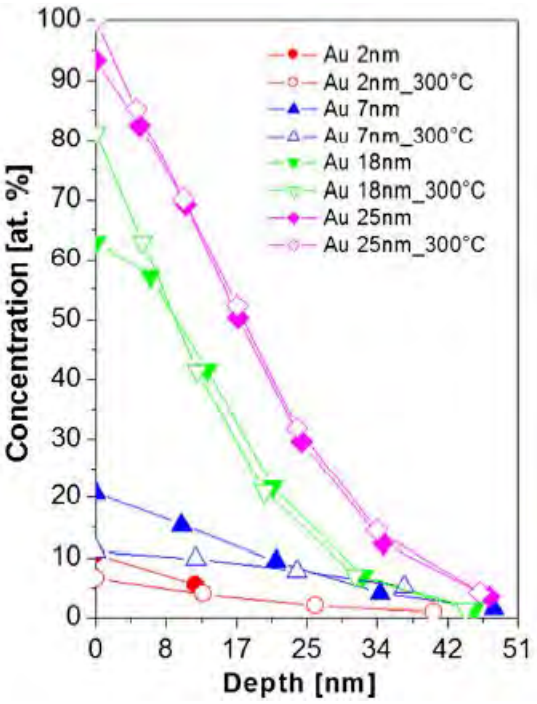

Figure 1 RBS spectra of gold structures evaporated on glass with room temperature and Au nanostructures evaporated on glass heated to 300°C (300°C).

PAPERS

1. A. Schaub, P. Slepička, I. Kašpárková, P. Malinský, A. Macková, V. Švorčík, *Gold nanolayer and nanocluster coatings induced by heat treatment and evaporation technique*, Nanoscale Res. Lett. 8 (2013) 249-257.

2. P. Slepička, P. Juřík, P. Malinský, A. Macková, N. Slepičková Kasálková, V. Švorčík, *Biopolymer nanostructures induced by argon plasma irradiation and metal sputtering*, NIM B, 2013, under review.

CONFERENCES

1. P. Slepička, P. Juřík, P. Malinský, A.Macková, N. Slepičková Kasálková, V. Švorčík, *Biopolymer nanostructures induced by argon plasma irradiation and metal sputtering*, IBA 2013 (Ion Beam Analysis), 23.6.-28.6. 2013, Seattle, USA.

2. N. Slepičková Kasálková, P. Slepička, P. Malinský, A. Macková, V. Švorčík, *Surface chamges of biopolymers induced by plasma treatment and acetone etching*, IBA 2013 (Ion Beam Analysis), 23.6.-28.6. 2013, Seattle, USA

NDP Experiment Time Application

Neutron Physics Laboratory - Nuclear analytical methods with neutrons

Xin Yang

Proposal ID

66

There are two samples have been measured by NDP, a natural boron coating on the silicon matrix sample and a LiF(natural Li) coating on the silicon matrix.

The measurement was performed in UHV chamber using the Hamamatsu detectors (8 × 8 mm^2) and distance from the sample 40 mm. The beam intensity was around $10^7/(cm^2s)$. The evaluation is based on the comparison with the B standard NDP pattern

The NDP spectrum are shown in Fig.1.

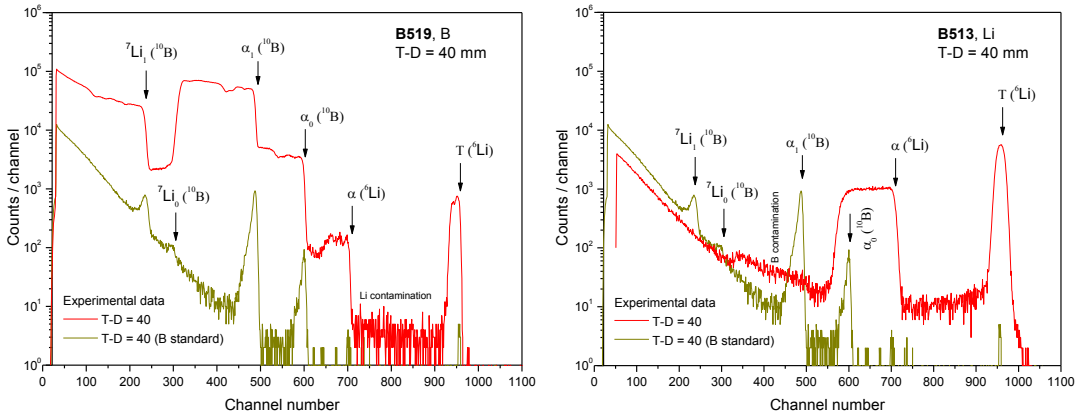

Fig 1. The spectrum of samples

The B sample is very inhomogeneous and contaminated by Li. The LiF sample looks relatively OK with a smooth alpha line platform and also be contaminated by B.

Profile results are shown in Fig 2.

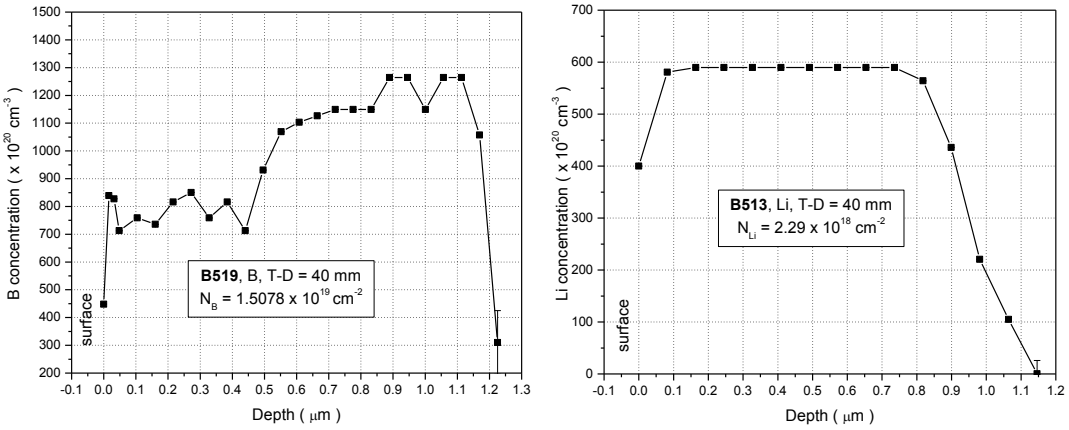

Fig 2. Profile of ^{10}B and ^7Li

The research has been conducted at the CANAM (Center of Accelerators and Nuclear Analytical Methods LM2011019) infrastructure with a funding from the Ministry of Education, Youth and Sports of the Czech Republic.

Cross section measurements of deuteron induced reactions

Laboratory of Cyclotron and Fast Neutron Generators

Eva Šimeková

Proposal ID

48

The proton and deuteron induced reactions are of a great interest for the assessment of induced radioactivity of accelerator components, targets and beam stoppers. Continuing our previous deuteron activation measurements on Al, Cu, Fe and Co, we measured excitation functions of reactions on Mn, Cr, W and Zr provoked by deuterons up to 20 MeV in three irradiations.

6.2.2013
We realized two runs. In the first one a Cr foil (together with Al foils serving for beam energy attenuation and as an additional monitor) was irradiated by deuteron with initial energy 19.76 MeV during 5 min with a mean current 0.15 μA. The stacked–foil activation technique was utilized to irradiate Mn foils (initial deuteron beam energy 19.76 MeV, irradiation time 5 min, mean current 0.32 μA) in the second run. The excitation function for 55Mn(d,p)56Mn 55Mn(d,2np+)54Mn and 55Mn(d,4np+)52Mn were provided for the deuteron energy range 2-20 MeV.

28.8.2013
Two runs were realized. It was performed a run (initial deuteron energy 20.09 MeV, similar condition as 6.2.2013) to irradiate single Cr foil and a stacked-foil activation technique was utilized to irradiate W foils in the second run. The foil activities measured by two HPGe detectors are processed now.

9.10.2013
Two runs were realized. It was performed a run (initial deuteron energy 20.025 MeV, similar condition as 6.2.2013) to irradiate single Cr foil and a stacked-foil activation technique was utilized to irradiate Zr foils in the second run. The activity measurements are proceeded to obtain values for long living isotopes.

We obtained cross section values for for 48V, 49Cr 52mMn, 52Mn, 54Mn generated by deuteron induced reactions on Cr.

Neutron Spectrum Determination of p+Be Source Reaction for Irradiation Experiments

Laboratory of Cyclotron and Fast Neutron Generators

Milan Štefánik

Proposal ID

80

Title: **Neutron Spectrum Determination of p+Be Source Reaction for Irradiation Experiments**

Objectives: Measurement of neutron energy spectrum and fluence of p+Be source reaction up to 34 MeV

The novel high power p-Be white neutron source with neutron energy range up to 34 MeV is currently in development at the NPI Řež. This was the first experimental run of newly upgraded beryllium target station of Department of Nuclear Reactions after the technical modification of the target station head (the reduction of the shell that should led to increase the value of neutron flux). After upgrade of Be-target station, it is possible to put the irradiated samples closer to the neutron source target and thus to obtain the higher neutron flux at the position of irradiated samples. In this technical test, the neutron spectrum is determined by the dosimetry foils method in the energy range of 0.1–34 MeV.

In the irradiation experiment, the multi-foil activation technique was used to determine the neutron spectrum of the p(35)-Be source reaction at the position of irradiated samples. The set of 10 activation foils (Al, Mn, Lu, Y, Ti, Co, Bi, Fe, Au, and In) with a diameter of 15 mm and with a thicknesses in the range of 0.05 mm to 0.5 mm was irradiated at the close target-to-sample position, where the high intensity neutron flux suitable for neutron activation experiments is expected. The selected activation foils of particular materials were sensitive to various energy part of neutron spectrum according to the activation cross-sections. For the continuous neutron spectrum production at the thick Be-target, the proton beam with an energy of 35 MeV and intensity of 10 microA was used. According to Monte Carlo prediction, the neutron flux up to 10^10 neutrons/s/cm2 at the position of activation foils should be achievable – this fact should be confirmed at the end of the experimental data processing for this experimental run. After the irradiation, in dependence on half-life periods of nuclear reaction products, the activation detectors of the large dosimetry foils set were repeatedly investigated be means of nuclear gamma-spectrometry technique – gamma-spectra measurement of daughter nuclei by the semiconductor HPGe detector. Now, the gamma-spectra of the most nuclear reaction products were measured; several long-life products still remains to be measured to obtain good statistical precision. The data processing of measured activation foils has just beginning and is under process and once it will be done, the neutron spectrum reconstruction in unfolding code SAND-II with apriory information form the MCNPX simulation and measured reaction rates will be performed, and thus the neutron field at the position of irradiated samples of the newly improved Be-target will be obtained.

Structural transitions in novel cobaltates Ln0.3CoO2 (Ln = La, Pr, and Nd)

Neutron Physics Laboratory - Neutron diffraction

Karel Knížek

Proposal ID

150

Structural study of layered cobaltate $La_{x/3}CoO_2$ ($x \sim 1$).

K. Knížek[1], Z. Jirák[1], J. Hejtmánek[1], J. Buršík[2], M. Soroka[2], and P. Beran[3]
[1] *Institute of Physics ASCR, Cukrovarnická 10, 162 00 Prague 6, Czech Republic.*
[2] *Institute of Inorganic Chemistry ASCR, 250 68 Řež near Prague, Czech Republic.*
[3] *Nuclear Physics Institute ASCR, 250 68 Řež near Prague, Czech Republic.*

Layered cobaltates of the Na_xCoO_2 type appeared suitable electronic materials for thermoelectric applications, especially in the range of a heavy hole doping $x \sim 0.70$ (~ 0.30 holes per Co). Recently, the systems $Ln_{x/3}CoO_2$ with trivalent Ln = La, Pr and Nd ions were successfully synthesized, starting from Na_xCoO_2 [1,2]. The Seebeck coefficient remains high as in the parent phase except for low temperatures $T < 50$ K, where a change from the positive to negative sign takes place abruptly. Before attempting any interpretation of such anomalous behavior, the $Ln_{x/3}CoO_2$ crystal structure and its temperature evolution have to be known in more detail.

The basic hexagonal structure of $La_{x/3}CoO_2$ characterized by $P6_3/mmc$ space group is similar to that of Na_xCoO_2, *i.e.* it is composed of layers of edge-sharing CoO_6 octahedra (the CoO_2 hexagonal sheets), separated by La monolayers. In distinction to Na_xCoO_2, La cation are ordered over one third of positions available originally for sodium, forming thus a $\sqrt{3}a_H \times \sqrt{3}a_H$ superstructure, in which the occupation of neighboring positions is avoided due to a strong electrostatic repulsion of trivalent La cations. This superstructure is reflected in diffraction patterns by highly asymmetric extra peaks with a sharp edge from the low 2θ side of the calculated position for superstructure lines (the most prominent are $\frac{1}{3}\frac{1}{3}0$ and $\frac{2}{3}\frac{2}{3}0$), and a long tail to higher 2θ. The shape of the peaks, together with a apparent absence of superstructure peaks with $l \neq 0$, is a strong signature that the ordering is only of a 2-dimensional character within *ab*-plane, without long range correlation along the *c*-axis.

Neutron diffraction patterns are exemplified by scans at 5 and 300 K in Fig. 1. Regarding the sudden change of Seebeck coefficient observed around 50 K, we have detected no significant change in neither structural nor lattice parameters around this temperature. The nature of this transition thus remains open, and we may only speculate that it might be related to a change of hole carrier dynamics or cobalt charge disproportionation.

TABLE I: Structural parameters and selected bond lengths and angles of $La_{x/3}CoO_2$ refined by Rietveld method within the hexagonal space group $P6_3/mmc$. Atom coordinates: La 2d(2/3,1/3,1/4), Co 2a(0,0,0), O 4f(1/3,2/3,z).

	5 K	300 K
a (Å)	2.8319(2)	2.8337(3)
c (Å)	11.110(1)	11.123(1)
La, B_{iso} (Å^2)	0.13(5)	0.17(5)
Co, B_{iso} (Å^2)	0.60(6)	0.59(6)
O, B_{iso} (Å^2)	0.15(2)	0.40(2)
O (z)	0.0910(4)	0.0914(4)
La, occupation	0.33(2)	0.33(2)
Co - O (Å) ×6	1.922(2)	1.926(2)
La - O (Å) ×6	2.407(3)	2.406(3)
O - Co - O (deg)	94.8(2)	94.7(2)
O - La - O (deg)	71.8(2)	72.1(2)

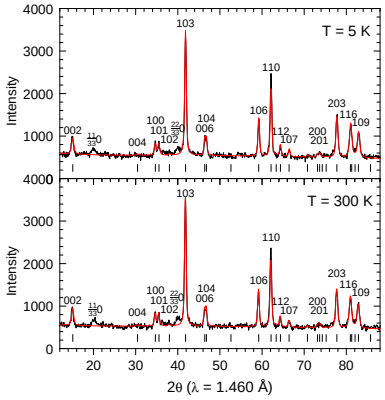

FIG. 1: Neutron diffraction patterns measured at temperatures 5 and 300 K. The main peaks of basic structure and superstructure (fractional indexes) are indicated.

The thermal expansion coefficients of $La_{x/3}CoO_2$ are practically equal in the *a* and *c* directions. This is in striking contrast to thermal expansion of the parent compound Na_xCoO_2, which is very anisotropic as regards the *a* and *c* directions. This distinct behavior may be explained by a different character of bonds between CoO_2 layers. The Na^+-O^{2-} bonds in Na_xCoO_2 have basically ionic character, they are weaker than the covalent Co-O bonds within the CoO_2 layers, and their thermal expansion is higher. Therefore the thermal expansion in *a*-direction is small since it is restricted by strong Co-O bonds, whereas large thermal expansion in *c*-direction is allowed by weak Na^+-O^{2-} bonds. The La^{3+}-O^{2-} bonds in $La_{x/3}CoO_2$ have relatively more covalent character than the Na^+-O^{2-} bond, and in addition, they are stronger because of the larger charge difference between La^{3+} and O^{2-}. Moreover, the LaO_6 prismatic coordination is strongly elongated with respect to the ideal trigonal prism defined by a model of six oxygen atoms in direct contacts. The bond angles O - La - O deviated to 72.0° and 94.5° from the ideal value 81.8°, which corresponds to an elongation of the LaO_6 prism along the trigonal axis by factor 1.25.

Inspection of the structural parameters in Table I. reveals, that the principal changes are an expansion of the Co-O bonds and a relaxation of the O-Co-O and O-La-O angles towards ideal values of octahedra (90°) and prism (81.8°), respectively. On the other hand, the La-O bonds remain constant within the error of measurement. Since an elongation of the La-O bonds itself would result in reducing the O-La-O angle, it is evident that the tendency to enlarge the O-La-O angle in order to attain the ideal prismatic coordination is the decisive factor for the evolution of LaO_6 coordination with temperature, and it outweighs the thermal expansion of La-O bonds.

[1] K. Knížek, *et al.*, J. Sol. St. Chem. **184**, 2231 (2011).
[2] K. Knížek, *et al.*, J. Appl. Phys. **111**, 07D707 (2012).